J Mater Sci (2015) 50:2522–2531
DOI 10.1007/s10853-014-8811-1

Influence of age on the free-radical scavenging ability of CeO_2 and Au/CeO_2 nanoparticles

M. Anandkumar · C. H. Ramamurthy · C. Thirunavukkarasu · K. Suresh Babu

Received: 17 October 2014 / Accepted: 22 December 2014 / Published online: 7 January 2015

Abstract Cerium oxide (CeO_2) nanoparticles have been demonstrated as a potential free-radical scavenger. In the present work, gold (Au) nanoparticles were impregnated by deposition precipitation method on the surface of the combustion synthesized 13-nm CeO_2 nanoparticles in order to enhance the free-radical scavenging properties of Au-supported CeO_2 nanoparticles (Au/CeO_2). Raman spectroscopic calculation for CeO_2 and Au/CeO_2 showed an oxygen vacancy concentration of 1.22×10^{21} and 0.80×10^{21} cm^{-3}, respectively. The dose- and time-dependent free-radical quenching efficacy of CeO_2 and Au/CeO_2 nanoparticles was evaluated against hydroxyl, superoxide and nitric oxide using in vitro method. CeO_2 and Au/CeO_2 nanoparticles exhibited efficient scavenging of hydroxyl and superoxide radicals, but the activity was found to be low against nitric oxide radicals. Both the nanoparticles exhibited a concentration-dependent free-radical scavenging in the range of 0.01–0.0001 μM and showed a saturation behaviour above 0.1 μM. Nanoparticle solution aged for 1, 7, 14 and 28 days displayed a lower superoxide and hydroxyl radicals scavenging activity compared to freshly prepared nanoparticle solution while nitric oxide exhibited the opposite behaviour. In comparison, Au/CeO_2 showed better radical scavenging activity at lower concentrations than that of CeO_2. The observed radical scavenging property can be attributed to the agglomeration as well as changes in surface oxygen vacancy concentration which are important in designing therapeutic agent for oxidative stress complications.

M. Anandkumar · K. S. Babu (✉)
Centre for Nano Sciences and Technology, Madanjeet School of Green Energy Technologies, Pondicherry University, Kalapet, Puducherry 605 014, India
e-mail: sureshbabu.nst@pondiuni.edu.in

C. H. Ramamurthy · C. Thirunavukkarasu
Department of Biochemistry and Molecular Biology, Pondicherry University, Kalapet, Puducherry 605 014, India

Introduction

Free radicals are atoms, molecules or ions having unpaired electrons, which are present in physiological systems and participate in many important metabolic processes including cell signalling. Since free radicals are highly reactive and less stable, they tend to react with other cellular components resulting in cell injury and premature cell death. Free radicals are classified into reactive oxygen species (ROS) and reactive nitrogen species (RNS). ROS includes hydrogen peroxide (H_2O_2), superoxide (O_2^-) and hydroxyl ($OH^\cdot$) which are derivatives of molecular oxygen (O_2). Although nitric oxide ($NO^\cdot$) plays an important role in physiology and regulation, it may lead to the formation of peroxy nitrite ($ONOO^-$) which is an important RNS [1–3]. The imbalance between the above-mentioned radical's generation and elimination may lead to various health issues including cancer [4]. Cerium oxide (CeO_2) nanoparticles exhibit unique redox property due to the existence of cerium in +3 and +4 oxidation states. Also CeO_2 switches between Ce^{3+} and Ce^{4+} in a reversible manner in response to the external reaction conditions. Due to the modifications in oxidation state of CeO_2, oxygen vacancies or defects are generated in the lattice structure by the loss of oxygen and/or its electrons to compensate the charges [5]. When Ce^{4+} reduces to Ce^{3+}, oxygen vacancies are generated that can be represented by the following Kroger–Vink notation,

$$O_o^x + 2Ce_{Ce}^x \leftrightarrow V_o^{\cdot\cdot} + 2Ce_{Ce}^{'} + \frac{1}{2}O_2 \quad (1)$$

where O_o^x is a neutral oxygen on an oxygen lattice site and Ce_{Ce}^x is a neutral cerium on a neutral cerium site, $V_o^{\cdot\cdot}$ is a +2 oxygen vacancy and $Ce_{Ce}^{'}$ is a Ce^{3+} atom in a Ce^{4+} site giving it a net negative charge of −1. Defect structure of CeO_2 is dynamic and may change in response to size and external parameters such as oxidizing or reducing environment, thereby acting as an oxygen buffer to either store or supply oxygen. The fraction of oxygen vacancy and Ce^{3+} concentration increases when the particle size is less than 15 nm [6]. This phenomenon observed at the nanoscale has been utilized in many areas of applications including biology [7–11], energy [12] and catalysis [13]. Applications of CeO_2 nanoparticles in the field of nanomedicine have been demonstrated based on its ability to scavenge free radicals as well as for its biocompatibility [14, 15]. CeO_2 nanoparticles have been reported to exhibit protection against radiation induced damage through its antioxidant property [4, 7, 8]. Though different-sized/surface functionalized CeO_2 nanoparticles have been prepared by various methods and tested its free-radical quenching property against individual free-radical compound, it is important to study the effectiveness of the same-sized nanoparticles against various free radicals in order to realize the multi-radical environment in the physiological conditions.

Gold (Au) nanoparticles have been applied in various fields, for example, medicine [16, 17], catalysis [18, 19], radical scavenging [20], etc. The unique property of Au is its biocompatibility and size/shape-dependent optical property which is used for its targeted therapy. Further, many reports are available on the efficiency of CeO_2 nanoparticles for radical scavenging, however, not much investigation have been made on the combined Au and CeO_2 system [14, 15, 21]. Recently, Menchon et al. reported the effect of biocompatible Au-supported CeO_2 nanoparticles exhibiting antioxidant activity against hydrogen peroxide [22]. The antioxidant effect of Au-supported CeO_2 nanoparticles against harmful radicals such as hydroxyl, superoxide and nitric oxide needs to be investigated to explore the possibilities of these nanoparticles as therapeutic compound against oxidative stress-mediated injury. The present work focuses on the formulation of Au-supported CeO_2 nanoparticles and tested its hydroxyl, superoxide and nitric oxide radical scavenging capabilities through standard assays. Further concentration and influence of nanoparticles ageing on free-radical scavenging property were also investigated.

Experimental

Materials

Cerium nitrate hexahydrate (Sigma-Aldrich, 99.9 %), glycine (Fisher Scientific), hydrochloro auric acid (Loba Chemicals) and sodium borohydride (Sigma Aldrich) were used for the synthesis of both cerium oxide and gold-impregnated cerium oxide nanoparticles. For radical scavenging assay preparation, ferric chloride, 2-deoxy-2-ribose, Ethylenediaminetetraacetic acid (EDTA), hydrogen peroxide (H_2O_2), Trichloroacetic acid (TCA), Thiobarbituric acid (TBA), ascorbic acid, phenazine methosulfate (PMS), nitro blue tetrazolium (NBT), nicotinamide adenine dinucleotide (NADH) and sodium nitro prusside, Griess reagent was purchased from Himedia. Catechin (Sigma-Aldrich) is used as a standard.

Method

Synthesis of CeO_2 nanoparticles

CeO_2 nanoparticles were synthesized by simple chemical combustion method using glycine as a fuel. Cerium nitrate and glycine (molar ratio of cerium nitrate to glycine 1:1.2) dissolved in the double-distilled water was stirred together until the formation of clear solution. The solution was kept in a hot plate and evaporated to form the dry powder. Subsequently, the mixture was heated at 300 °C to initiate the ignition of fuel and oxidizer leading to the combustion reaction. The resultant powder was centrifuged and washed with double-distilled water for three times to remove unreacted nitrate and glycine and dried in an oven overnight to obtain CeO_2 nanoparticles.

Gold-supported CeO_2 nanoparticles

Au-supported CeO_2 nanoparticles (Au/CeO_2) were synthesized by simple deposition precipitation method. CeO_2 nanoparticles dispersed in water were added drop wise with stirring into $HAuCl_4$ solution and subsequently dried at 100 °C. The resultant powder was then redispersed in distilled water and the required amount of $NaBH_4$ was added drop wise until the reduction of gold salt to gold nanoparticles. The solution was centrifuged, washed with double distilled water and dried in hot air oven overnight. The stoichiometry of Au to CeO_2 was maintained in such a manner in order to obtain 3.5 weight percentage of Au over CeO_2.

Characterization

X ray diffraction (XRD) studies were performed using Rigaku Ultima IV diffractometer using Cu K_α radiation with a scan rate of 4° per min for CeO_2 and Au/CeO_2 in the range of 25–50°. Surface morphological and elemental analysis of the nanoparticle was performed using with Carl Zeiss Supra 40 Field Emission Scanning Electron Microscope (FESEM) operated at 20 kV. Optical analysis was

carried out using Perkin Elmer Lambda 650S UV Visible Spectrometer. Raman spectra were recorded using Reinshaw Laser confocal Raman Microscope RM 2000 with spectrometer. The sample was excited using a 514 nm Ar^+ laser with a power of 0.5 % exposed for 30 s with the beam diameter of 1 μm on the sample and data collected at an interval of 1 cm^{-1}. Particle size distribution of nanoparticles of fresh and 28-day-aged samples (0.1 mM) were carried out using Malvern Zetasizer.

Hydroxyl radical scavenging assay

Hydroxyl radical scavenging property of nanoparticle was analysed by Halliwell et al. [23]. The assay is based on quantification of the degradation product of 2-deoxyribose by condensation with TBA. Hydroxyl radical was generated by Fenton reaction (The reaction mixture consists of $FeCl_3$, ascorbate, EDTA and H_2O_2). The final reaction volume of 1 ml contains 2.8 mM 2-deoxy-2-ribose, 20 mM pH 7.4 KH_2PO_4–KOH buffer, 100 μM $FeCl_3$, 100 μM EDTA, 1.0 mM H_2O_2, 100 μM ascorbic acid with varying concentrations of nanoparticles. From the nanoparticle, stock solutions of 1000 μM various dilutions were made to obtain the final concentration of 0.0001, 0.001, 0.01, 0.1, 1, 10 and 100 μM. The reaction mixture was incubated for 1 h at 37 °C. 1 ml of 2.8 % TCA was added to arrest the reaction. Chromogenic adduct was formed by adding 1 ml of 1 % aqueous TBA and incubated at 90 °C for 15 min. The intensity of chromogen was measured at 532 nm against an appropriate blank solution. Catechin (10 μM) was used as a positive control.

Hydroxyl radicals have been generated by iron-EDTA complex with H_2O_2 in the presence of ascorbic acid.·OH radicals generated by the above reaction decomposes deoxyribose. The prevention of deoxyribose degradation determines the hydroxyl scavenging property. The scavenging (% inhibition) of ·OH by nanoparticles was calculated based on the formula given in Eq. (2).

$$\%\,\text{Inhibition} = \frac{A_{\text{control}} - A_{\text{test}}}{A_{\text{control}}} * 100 \qquad (2)$$

where A_{control} is the activity in the absence of nanoparticle and A_{test} is the activity in the presence of nanoparticle.

Superoxide radical scavenging assay

Superoxide radical assay was performed by following Nishikimi et al. [24]. The reaction mixture contains 1 ml of 156 mM NBT, 1 ml of 468 mM NADH and 1 ml of corresponding nanoparticles. The reaction was started by adding 100 μl of 60 mM PMS. NBT, NADH and PMS solution were prepared using phosphate buffer (pH 7.4). The reaction mixture was incubated at 25 °C for 15 min and the absorbance was measured at 560 nm against blank sample. Catechin was used as a positive control. The scavenging (inhibition) of superoxide free radicals by nanoparticles was calculated according to Eq. (2).

Assay of nitric oxide radical quenching activity

The nitric oxide radical quenching activity was evaluated as per the procedure reported by Sousa et al. [25]. Nitric oxide radicals were generated using of 20 mM sodium nitro prusside solution. To 100 μl of this solution, various concentration of nanoparticles were added and incubated for 60 min at room temperature. 100 μl of Griess reagent were added subsequently to the mixture and incubated for 15 min. Catechin was used as a positive control. The inhibition of free radicals by nanoparticles was evaluated by Eq. (2).

Results and discussion

X-ray diffraction

The XRD pattern for CeO_2 and Au/CeO_2 is shown in Fig. 1. XRD data confirm the presence of cubic fluorite-structured CeO_2 consisting of (111), (200), (220) planes with the space group of $Fm\bar{3}$ m (ICDD Card Number: 01-073-6318). When Au was impregnated on the surface of CeO_2, new peaks at 2θ values of 38.08, 44.32° emerged which corresponds to (111), (200) planes of cubic Au (ICDD Card Number: 03-065-2870). The mean crystallite size of CeO_2 calculated using Scherrer's equation was found to be 13 nm. Calculation of Au nanoparticle size was

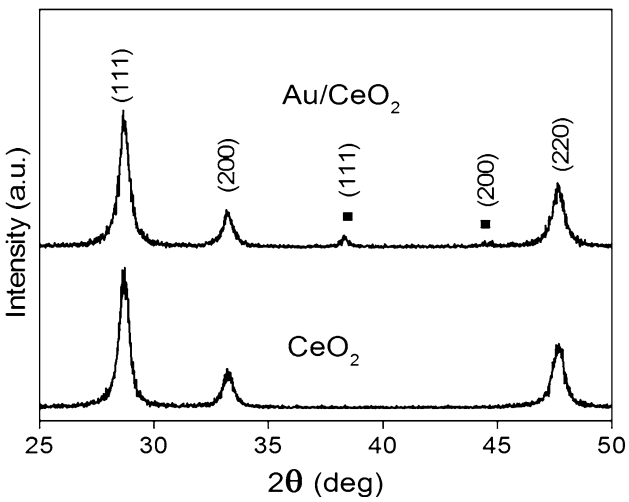

Fig. 1 X ray diffraction pattern of CeO_2 and Au/CeO_2 nanoparticles. ("*filled square*" denotes presence of Au peak)

found to be difficult due to low intensity of the XRD peaks. A similar observation of difficulty in detecting less than 4-nm-sized Au nanoparticle in XRD was reported by A-boukaïs et al. for Au/CeO_2 system deposited through deposition–precipitation method [26]. The calculated lattice parameter was found to be 0.5392 nm for the as prepared CeO_2 nanoparticle which is smaller than the bulk CeO_2 value (0.541 nm). The observed decrease in lattice parameter can be attributed to the experimental conditions as well as the nature of fuel used for the synthesis [27].

Scanning electron microscopy

Surface morphology of CeO_2 and Au/CeO_2 is shown in Fig. 2a, b and the corresponding EDX data in c and d, respectively. A porous network structure was observed for CeO_2 (Fig. 2a) due to the inherent nature of combustion process. Upon ignition, combustion process takes place which results in the generation of large volume of gases. The escape of generated gas during the combustion reaction, a porous network of nanostructure was obtained. Finely dispersed and few agglomerated bright spherical spots on the surface of CeO_2 nanoparticle were observed for Au/CeO_2 (Fig. 2b). Absence of these bright spots in the pure CeO_2 (Fig. 2a) indicates the presence of finely dispersed Au nanoparticle in Au/CeO_2. Since intensity of scattered electron is proportional to atomic number of the elements, Au appears brighter than Ce due to difference in atomic number. Figure 2c, d shows the EDS spectra of the samples CeO_2 and Au/CeO_2 which confirms the presence of gold in the later. EDS quantification of Au indicates the presence of 3.2 wt% of Au instead of the theoretical amount of 3.5 wt% due to the loss of weakly adsorbed Au during the washing of the sample.

UV visible spectroscopy

Optical absorption spectra of CeO_2 and Au/CeO_2 is shown in Fig. 3a, b, respectively. CeO_2 has an absorption band around 360 nm which can be attributed to the $Ce^{4+} \rightarrow O^{2-}$ charge transfer transitions [28]. In addition, for Au/CeO_2 nanoparticles, a new broad absorption band around

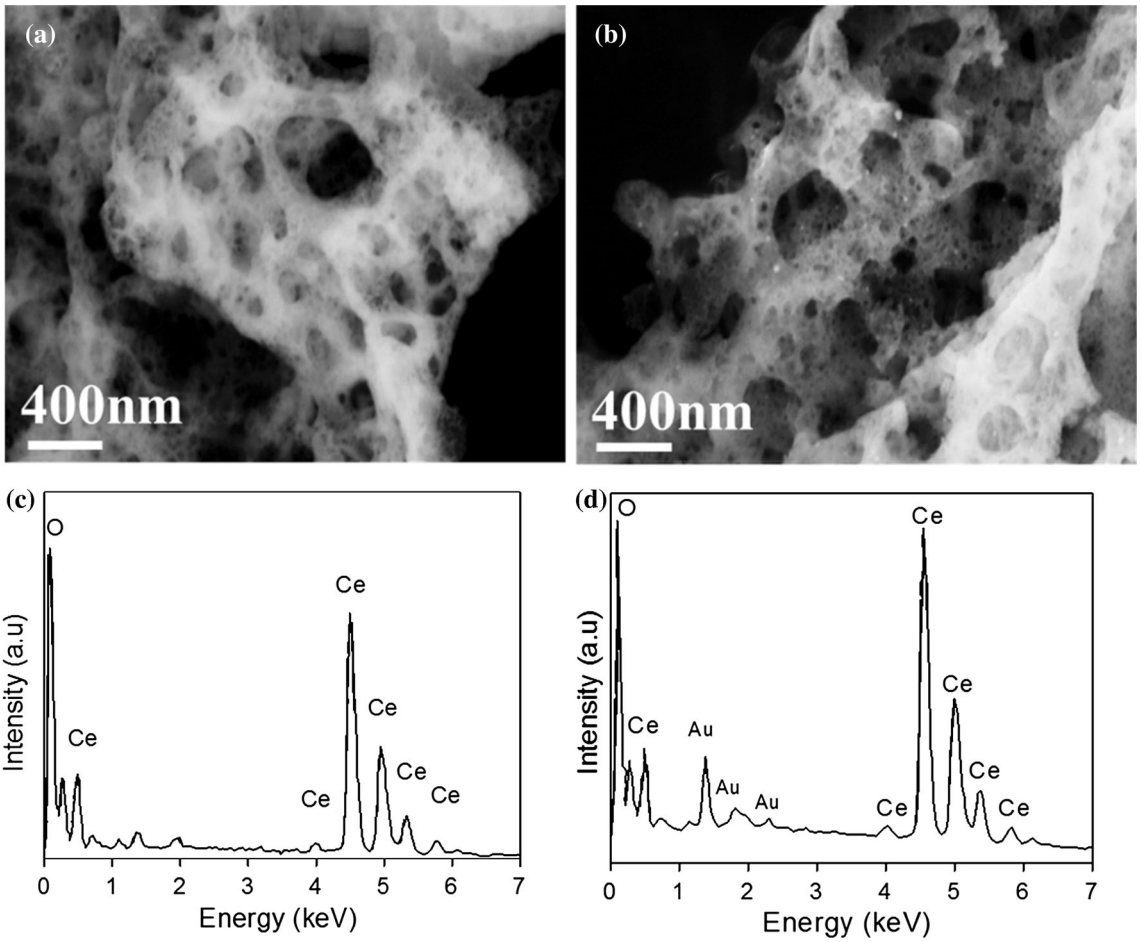

Fig. 2 SEM image of CeO_2 and Au/CeO_2 nanoparticles (**a** and **b**) and their corresponding EDS spectra (**c** and **d**)

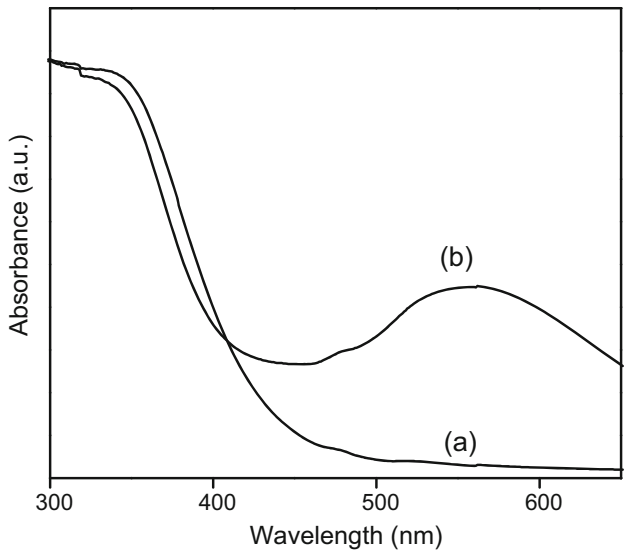

Fig. 3 UV Visible spectra of (*a*) CeO_2 and (*b*) Au/CeO_2 powders

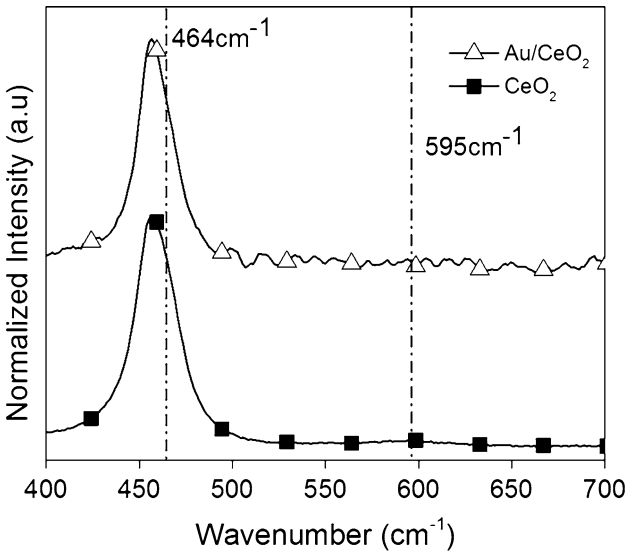

Fig. 4 Raman spectra of CeO_2 and Au/CeO_2 powders

500–650 nm with a maxima around 557 nm was observed. This new band upon Au coating on CeO_2 appears as a result of localized surface plasmon resonance (LSPR). When the incident photon frequency matches with the frequency of oscillation of surface electrons from Au nanoparticles LSPR appears [29]. The broadness of LSPR peak may be attributed to the size distribution of Au particles in Au/CeO_2. Based on the LSPR peak position, estimated gold size on CeO_2 surface may be less than 5 nm as reproted by Wei et al. [30].

Raman spectroscopy

Raman spectra recorded for CeO_2 and Au/CeO_2 powders are shown in Fig. 4. A symmetric peak around 464 cm^{-1} is generally observed in micron-sized CeO_2 which corresponds to Raman active vibrational mode of F2 g symmetric cubic fluorite structured CeO_2 [31]. In the present case, a broad asymmetric peak at a lower energy of 457 cm^{-1} was observed due to the presence of CeO_2 in the form of nanoparticles [32, 33]. In addition, a band around 595 cm^{-1} was observed due to the presence of Frenkel-type oxygen vacancies [32]. Upon impregnation of Au on the surface of CeO_2, the oxygen vacancy peak around 595 cm^{-1} diminishes due to the growth of Au nanoparticle on the vacancy sites of CeO_2 [34]. Spatial correlation model was used to quantify the oxygen vacancy concentration from Raman spectra [35–37] and was found to be 1.22×10^{21} and 0.80×10^{21} cm^{-3} for CeO_2 and Au/CeO_2, respectively. The presence of lower oxygen vacancy concentration in the case of Au/CeO_2 can be attributed to the interaction of Au atom with the vibration frequency of Ce–O matching with the observed surface morphology in SEM.

Effect of nanoparticle concentration on free-radical scavenging activity

Hydroxyl, superoxide, and nitric oxide radical scavenging property at the concentrations of 0.0001, 0.001, 0.1, 1, 10 and 100 μM for CeO_2 and Au/CeO_2 nanoparticles are shown in Fig. 5 a–f. The percent inhibition of free-radical formation increases with increasing nanoparticle concentration (0.0001 to 0.1 μM) which was found to be independent of the nature of radical being investigated. Above the critical concentration of 0.1 μM (found in the presents study), the percent inhibition was found to be in steady state for all the radicals. Xue et al. [7] studied the effect of hydroxyl radical scavenging with respect to CeO_2 concentration (0.1 to 0.001 μM) and found that scavenging efficiency depends on the concentration of nanoparticles. For hydroxyl radical scavenging in the presence of CeO_2 nanoparticles, inhibition increased from 0.6 % (0.0001 μM) to 11.2 % (0.1 μM). The percent inhibition was around 60 % at 1 μM and found to be better than the control (51 %) used in the present study. A similar trend was observed for Au/CeO_2 nanoparticles in hydroxyl radical scavenging except at 0.1 μM (15.4 %) concentration. For superoxide radical scavenging, inhibition increases from 0.2 % (0.0001 μM) to 10.1 % (0.1 μM) and saturated at about 47 % (from 1 μM onwards) which was found to be lower when compared to control (65 %). Compared to CeO_2, Au/CeO_2 nanoparticles showed a higher percentage of inhibition at lower concentrations (4.6 % at 0.001 μM and 15.7 % at 0.1 μM) compared to CeO_2 of similar concentration. In the case of nitric oxide both CeO_2 and Au/CeO_2 nanoparticles exhibited a similar trend where the percentage of inhibition increased from 0.2 % (0.0001 μM) to 7.5 % (0.1 μM) and saturated at about 32 % at higher

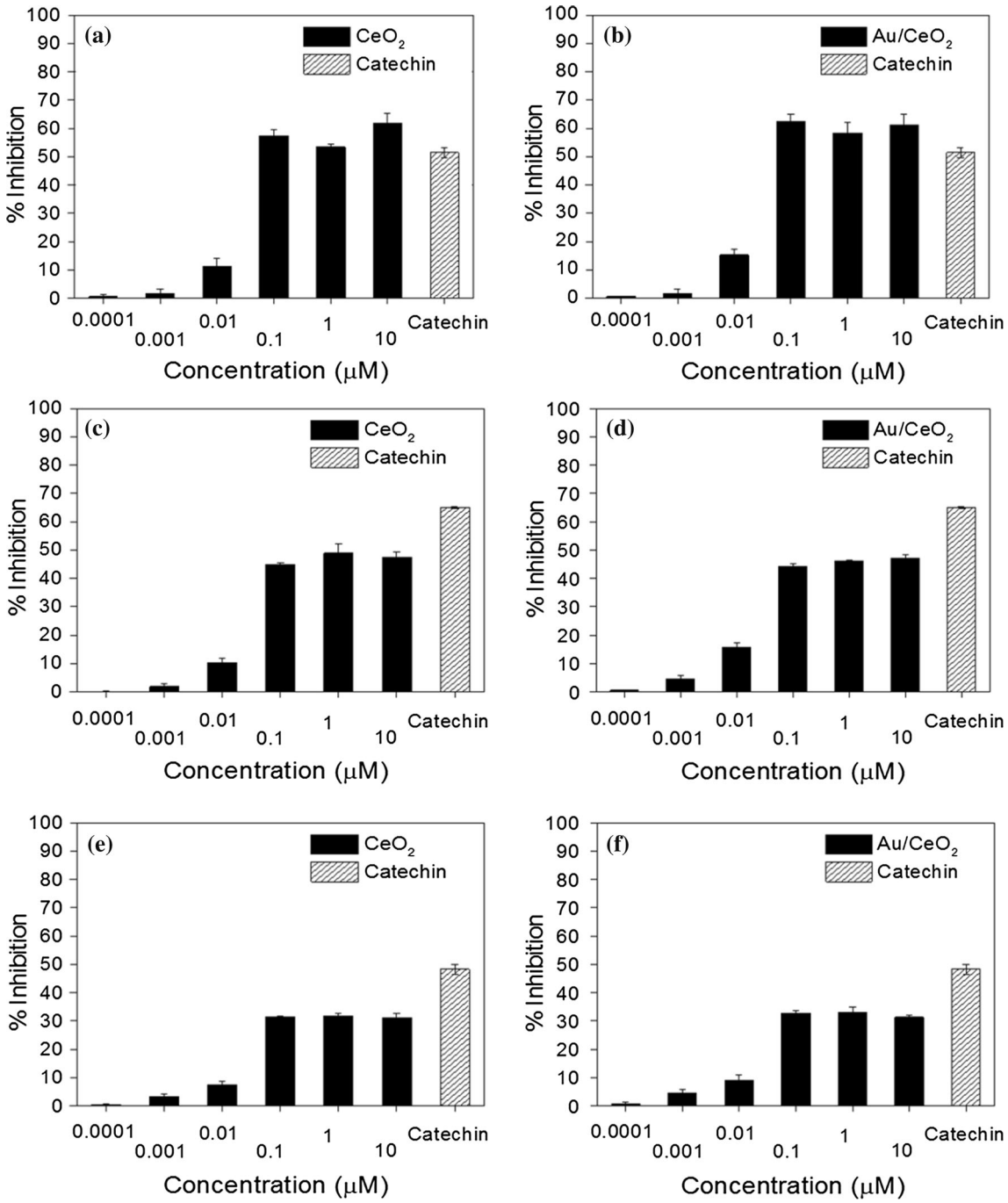

Fig. 5 Concentration-dependent **a**, **b** hydroxyl, **c**, **d** superoxide, and **e**, **f** nitric oxide radical scavenging effect of CeO_2 and Au/CeO_2 nanoparticles, respectively

concentrations indicating the lower activity compared to control (48 %). In comparison with control, both CeO_2 and Au/CeO_2 nanoparticles exhibited better inhibition property against hydroxyl radical while lower property in the presence of superoxide and lowest property against nitric oxide radicals.

The scavenging effect is due to the inherent property of CeO_2 where its oxidation state shifts between +3 and +4. On the formation of Ce^{3+}, oxygen vacancies are generated which act as active sites for the reaction with radicals. In the case of hydroxyl radical scavenging, it has been reported that CeO_2 active sites react only with $^{\cdot}OH$ and not with H_2O_2 which was used to generate these radicals [7]. Since the concentration of CeO_2 nanoparticle used was much lower than that of H_2O_2 (1 mM) to generate $^{\cdot}OH$, obviously the oxidation state (Ce^{3+}) and hence oxygen

vacancies were regenerated by the surface chemical reaction with ions such as H^+ present in the solution. The possible mechanism for hydroxyl radical scavenging can be represented as

$$Ce_2O_3 + 2^{\cdot}OH \rightarrow 2CeO_2 + H_2O \quad (3)$$

$$2CeO_2 + H^+(aq) \rightarrow Ce_2O_3 + {}^1/_2O_2 \quad (4)$$

As shown by Raman studies, CeO_2 and Au/CeO_2 differ in the concentration of oxygen vacancy though the same CeO_2 was used as the starting material for the formation of Au/CeO_2. Though Au/CeO_2 had 34 % lower oxygen vacancy concentration than that of CeO_2, it exhibited higher dose-dependent activity at lower concentration and inhibition activity equivalent to that of CeO_2 at higher concentrations. On account of the lower surface defect concentration, Au/CeO_2 was expected to show lower activity than that of CeO_2 which was contrary to the observed experimental trend. The radical scavenging activity may depend not only on the oxygen vacancy concentration of CeO_2 but also on the surface charge of Au. DFT calculation reported for Au/CeO_2 system indicates that the presence of Au as $Au^{\delta+}$ on the surface of CeO_2 converts Ce^{4+} to Ce^{3+} [38] leading to an increase in the concentration of Ce^{3+} and oxygen vacancy. Since in the present work Raman study shows a lower oxygen vacancy concentration for Au/CeO_2 compared to CeO_2, Au is likely to be present predominantly in the form of Au^o rather than $Au^{\delta+}$ as it would have increased the oxygen vacancy concentration. Above the critical concentration of 0.1 μM, Au has limited role to play and the concentration of oxygen vacancy in CeO_2 was sufficient enough to inhibit the radicals.

Figure 5c, d shows superoxide radical scavenging property of CeO_2 and Au/CeO_2, respectively. Up to 0.1 μM both CeO_2 and Au/CeO_2 exhibited concentration-dependent activity and exhibit a saturated behaviour above 0.1 μm. Korsvik et al. [39] showed that the presence of higher oxygen vacancy concentration is essential for the efficient degradation of superoxide. Since the concentration of nanoparticle is far lower than the concentration of superoxide generated, a single nanoparticle is efficient in degradation and gets regenerated as shown below:

$$2Ce_2O_3 + 2O_2^{\cdot -} \rightarrow 4CeO_2 + O_2 \quad (5)$$

$$4CeO_2 + H^+(aq) \rightarrow 2Ce_2O_3 + O_2 \quad (6)$$

The effect of CeO_2 and Au/CeO_2 on scavenging nitric oxide is shown in Fig. 5e, f. Both CeO_2 and Au/CeO_2 exhibited a lower nitric oxide inhibition activity when compared to that of hydroxyl and superoxide radical scavenging. Since transfer of an unpaired electron from nitric oxide to CeO_2 is the important step, presence of Ce^{4+} is necessary to enable the reduction to Ce^{3+} state after reduction [8]. In the present work, as CeO_2 contain high concentration of Ce^{3+} than Ce^{4+} in the freshly prepared condition, the efficiency was found to be lower. The mechanism of nitric oxide radical scavenging can be represented as,

$$2CeO_2 + NO^{\cdot} \rightarrow Ce_2O_3 + NO_2 \quad (7)$$

$$2Ce_2O_3 + 2OH^-(aq) \rightarrow 4CeO_2 + H_2O \quad (8)$$

Ageing effect of nanoparticles

CeO_2 nanoparticles exist dynamically in two oxidation states and there exists time-dependent conversion between Ce^{3+} and Ce^{4+} and vice versa. Since our earlier studies have shown that upon ageing agglomerate size increases with the change in oxidation state from +3 to +4, we carried out ageing studies to delineate the effect of oxidation state and radical scavenging activity. Three different concentrations (0.1, 1 and 10 μM) of CeO_2 and Au/CeO_2 were tested for hydroxyl, superoxide and nitric oxide radical scavenging with fresh, 1, 7, 14 and 28 days of aged samples. Figure 6a, b shows the hydroxyl radical scavenging property with respect to ageing time for CeO_2 and Au/CeO_2, respectively. Though freshly prepared nanoparticles showed a better inhibition property (about 50–60 %) at all concentrations than that of control, scavenging efficiency reduced with ageing time. After 28 days of ageing, nanoparticles were found to be assisting rather than inhibiting the radicals in a concentration-dependent manner. Compared to CeO_2, Au/CeO_2 showed better scavenging property in spite of ageing. Superoxide radical scavenging of CeO_2 and Au/CeO_2 nanoparticles (Fig. 6c, d) exhibited a time-dependent reduction in % of inhibition and turned to a minimum by about day 28. Contrary to the observation recorded in the case of superoxide and hydroxyl, nitric oxide radical scavenging showed a time-dependent increase in % of inhibition with a maximum of 42 % (Fig. 6e, f). As discussed above, for effective scavenging of hydroxyl and superoxide radicals more oxygen vacancy is required and a decrease in defect concentration decreases the percentage of inhibition. On the other hand, lower oxygen vacancy (higher Ce^{4+}) concentration is required for the scavenging of nitric oxide. Two factors which may have profound influence on the activity of radical scavenging can be agglomeration or oxygen vacancy concentration (or oxidation state of cerium).

The change in agglomeration of fresh and aged CeO_2 and Au/CeO_2 nanoparticles was evaluated by Zetasizer measurements as shown in Fig. 7. A freshly prepared nanoparticles exhibited an average hydrodynamic radii of 313 and 288 nm for CeO_2 and Au/CeO_2, respectively. Au/CeO_2 nanoparticle exhibited smaller radii compared to CeO_2. This may be due to the presence of Au on CeO_2

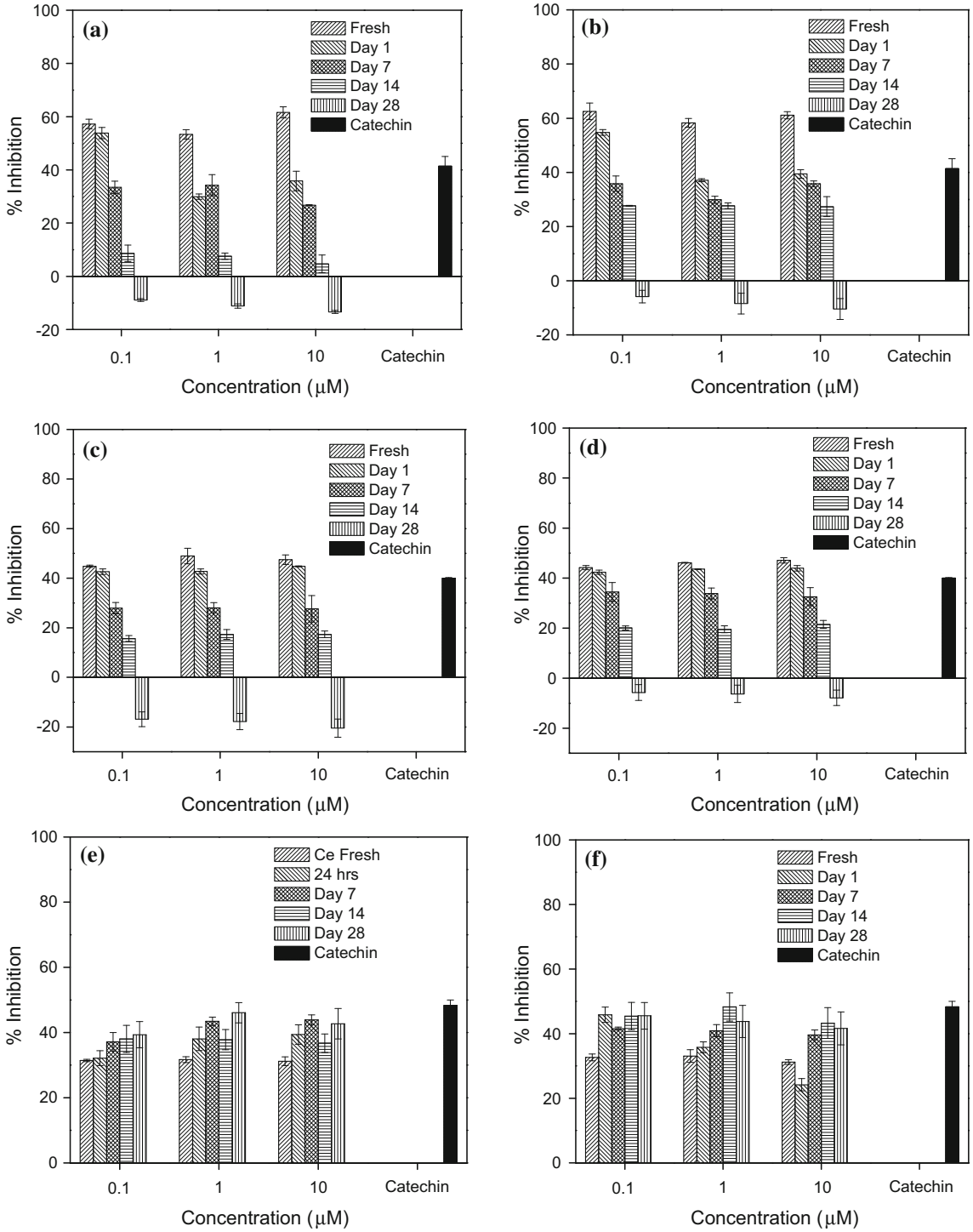

Fig. 6 Time-dependent free-radicals scavenging effect of CeO_2 and Au/CeO_2 nanoparticles

surface which prevents the nanoparticle agglomeration since Au is present as $Au^{\delta+}$ on the surface of CeO_2 [38, 40, 41]. During the course of ageing, after 28 days hydrodynamic radii of CeO_2 increased 313–415 nm. But in the case of Au/CeO_2 the particle size was found to be reduced to 213 nm. Though in the as prepared condition both CeO_2 and Au/CeO_2 have higher oxygen vacancy (or Ce^{3+}) concentration, upon ageing nanoparticle begins to agglomerate. If the overall oxygen vacancy concentration remains constant for a given concentration of nanoparticle, upon ageing the effective oxygen vacancy present on the surface decreases as a result of agglomeration. This is true

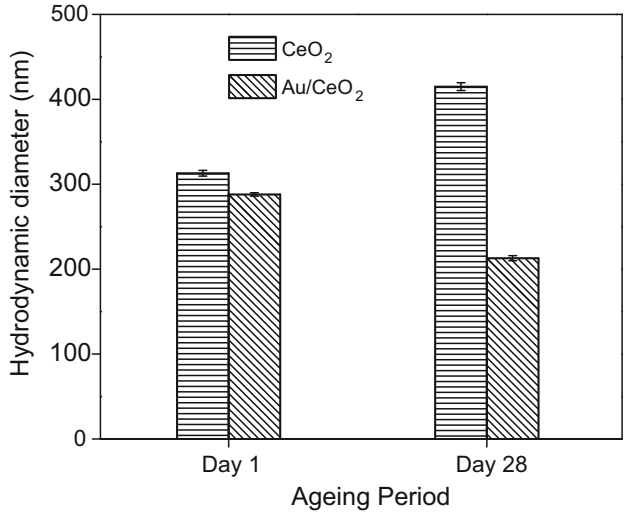

Fig. 7 Time-Dependent Zetasizer measurement of nanoparticle solution (0.1 mM)

for freshly prepared nanoparticle solution but upon ageing not only oxygen vacancy concentration, but agglomeration is also important as it changes the effective surface area which can modify the active sites available on the surface. Similar results were observed by Babu et al. [1] considering the effect of agglomeration on hydroxyl radical scavenging with CeO_2 nanoparticles. Kuchibhatla et al. [11] reported a transition from Ce +3 to +4 upon ageing. Agglomeration and oxidation lead to the reduction in observed inhibition activity for various radicals. The difference in agglomeration kinetics and radical scavenging between CeO_2 and Au/CeO_2 can be attributed to the kinetics which are responsible for colloidal stability as Au present on the surface reduces the agglomeration. Upon ageing growth of CeO_2 nanoparticles leads to a decrease in activity for superoxide and hydroxyl radicals.

Conclusions

In summary, Au-coated CeO_2 nanoparticles were synthesized by deposition precipitation technique which resulted in the fine dispersion of Au on the surface of CeO_2 nanoparticles. Their radical quenching efficacy was evaluated with different types of assays with concentration-dependent as well as ageing of nanoparticle solution. Results suggest that saturation of inhibition activity occurs in all assays proving that at larger concentration of nanoparticle reduces the accessibility to active sites due to agglomeration. Also ageing studies proved that agglomeration and oxidation of Ce^{3+} to Ce^{4+} increase the nitric oxide scavenging ability whereas decrease hydroxyl and superoxide radical inhibition. The present finding will be helpful in future drug delivery applications where the stability of nanoparticle is very important.

Acknowledgements Authors gratefully acknowledge the funding support from Start Up Grant (PU/PC/Start-up Grant/2011-12/312) provided by Pondicherry University, India as well as Indian Council of Medical Research (ICMR Ref: 52/13/2007) and Department of Science and Technology (NO.SR/FT/LS-63/2011), New Delhi, India. The authors wish to thank Central Instrumentation Facility (CIF), Pondicherry University for the characterization.

References

1. Babu S, Velez A, Wozniak K, Szydlowska J, Seal S (2007) Electron paramagnetic study on radical scavenging properties of ceria nanoparticles. Chem Phys Lett 442:405–408
2. Karakoti AS, Singh S, Kumar A, Malinska M, Kuchibhatla SVNT, Wozniak K, Self WT, Seal S (2009) PEGylated nanoceria as radical scavenger with tunable redox chemistry. J Am Chem Soc 131:14144–14145
3. Karakoti AS, Singh S, Dowding JM, Seal S, Self WT (2010) Redox-active radical scavenging nanomaterials. Chem Soc Rev 39:4422–4432
4. Wason MS, Colon J, Das S, Seal S, Turkson J, Zhao J, Baker CH (2013) Sensitization of pancreatic cancer cells to radiation by cerium oxide nanoparticle-induced ROS production. Nanomedicine: nanotechnol. Biol Med 9:558–569
5. Babu S, Schulte A, Seal S (2008) Defects and symmetry influence on visible emission of Eu doped nanoceria. Appl Phys Lett 92(123112):1–3
6. Wu L, Wiesmann HJ, Moodenbaugh AR, Klie RF, Zhu Y, Welch DO, Suenaga M (2004) Oxidation state and lattice expansion of CeO_{2-x} nanoparticles as a function of particle size. Phys Rev B 69(125415):1–9
7. Xue Y, Luan Q, Yang D, Zhou K (2011) Direct evidence for hydroxyl radical scavenging activity of cerium oxide nanoparticles. J Phys Chem C 115:4433–4438
8. Dowding JM, Dosani T, Kumar A, Seal S, Self WT (2012) Cerium oxide nanoparticles scavenge nitric oxide radical ($^{\bullet}NO$). Chem Commun 48:4896–4898
9. Pelletier DA, Suresh AK, Holton GA, McKeown CK, Wang W, Gu B, Mortensen NP, Allison DP, Joy DC, Allison MR, Brown SD, Phelps TJ, Doktycz MJ (2010) Effects of engineered cerium oxide nanoparticles on bacterial growth and viability. Appl Environ Microbiol 76:7981–7989
10. Lorda MS, Jung MS, Teoh WY, Gunawan C, Vassie JA, Amal R, Whitelock JM (2012) Cellular uptake and reactive oxygen species modulation of cerium oxide nanoparticles in human monocyte cell line U937. Biomaterials 33:7915–7924
11. Kuchibhatla SVNT, Karakoti AS, Baer DR, Samudrala S, Engelhard MH, Amonette JE, Thevuthasan S, Seal S (2012) Influence of aging and environment on nanoparticle chemistry: implication to confinement effects in nanoceria. J Phys Chem C 116:14108–14114
12. Arunkumar P, Meena M, Babu KS (2012) A review on cerium oxide-based electrolytes for ITSOFC. Nanomater Energy 1:288–305
13. Osawa T, Nakai Y, Mouri A, Lee IYS (2013) Studies of the preparation method of ceria-promoted nickel catalyst for carbon dioxide reforming of methane. Appl Catal A 474:100–106
14. Perez JM, Asati A, Nath S, Kaittanis C (2008) Synthesis of biocompatible dextran-coated nanoceria with pH-dependent antioxidant properties. Small 4:552–556

15. Lee SS, Song W, Cho M, Puppala HL, Nguyen P, Zhu H, Segatori L, Colvin VL (2013) Antioxidant properties of cerium oxide nanocrystals as a function of nanocrystal diameter and surface coatings. ACS Nano 7:9693–9703
16. Lal S, Clare SE, Halas NJ (2008) Nanoshell-enabled photothermal cancer therapy: impending clinical impact. Acc Chem Res 41: 1842–1851
17. Anker JN, Hall WP, Lyandres O, Shah NC, Zhao J, Duyne RPV (2008) Biosensing with plasmonic nanosensors. Nat Mater 7:442–453
18. Fan C, Zhang L, Wang S, Wang D, Lu L, Xu A (2012) Novel CeO_2 yolk-shell structures loaded with tiny Au nanoparticles for superior catalytic reduction of p-nitrophenol. Nanoscale 4:6835–6840
19. Zhang J, Chen G, Chaker M, Rosei F, Ma D (2013) Gold nanoparticle decorated ceria nanotubes with significantly high catalytic activity for the reduction of nitrophenol and mechanism study. Appl Catal B 132:107–115
20. Ramamurthy CH, Padma M, Samadanam IDM, Mareeswaran R, Suyavaran A, Sureshkumar M, Premkumar K, Thirunavukkarasu C (2013) The extra cellular synthesis of gold and silver nanoparticles and their free radical scavenging and antibacterial properties. Colloids Surf B 102:808–815
21. Vincent A, Inerbaev TM, Babu S, Karakoti AS, Self WT, Masunov AE, Seal S (2010) Tuning hydrated nanoceria surfaces: experimental/theoretical investigations of ion exchange and implications in organic and inorganic interactions. Langmuir 26: 7188–7198
22. Menchón C, Martín R, Apostolova N, Victor VM, Alvaro M, Herance JR, García H (2012) Gold nanoparticles supported on nanoparticulate ceria as a powerful agent against intracellular oxidative stress. Small 8:1895–1903
23. Halliwell B, Gutteridge JMC, Aruoma OI (1987) The deoxyribose method: a Simple, "test-tube" assay for determination of rate constants for reactions of hydroxyl radicals. Anal Biochem 165:215–219
24. Nishikimi M, Rao NA, Yagi K (1972) The occurrence of superoxide anion in the reaction of reduced phenazine methosulfate and molecular oxygen. Biochem Biophys Res Commun 46:849–854
25. Sousa C, Valentão P, Ferreres F, Seabra RM, Andrade PB (2008) Tronchuda cabbage (*Brassica oleracea* L. var. costata DC): scavenger of reactive nitrogen species. J Agric Food Chem 56: 4205–4211
26. Aboukaïs A, Aouad S, El-Ayadi H, Skaf M, Labaki M, Cousin R, Abi-Aad E (2012) Physicochemical characterization of Au/CeO_2 solid. Part 1: the deposition-precipitation preparation method. Mat Chem Phys 137:34–41
27. Gu L, Meng G (2007) Powder synthesis and characterization of nanocrystalline CeO_2 via the combustion processes. Mater Res Bull 42:1323–1331
28. Taguchi M, Takami S, Adschiri T, Nakane T, Sato K, Naka T (2011) Supercritical hydrothermal synthesis of hydrophilic polymer-modified water-dispersible CeO_2 nanoparticles. Cryst Eng Comm 13:2841–2848
29. Kominami H, Tanaka A, Hashimoto K (2011) Gold nanoparticles supported on cerium (IV) oxide powder for mineralization of organic acids in aqueous suspensions under irradiation of visible light of $\lambda = 530$ nm. Appl Catal A 397:121–126
30. Wei Y, Liu J, Zhao Z, Duan A, Jiang G (2012) The catalysts of three-dimensionally ordered macroporous $Ce_{1-x}Zr_xO_2$-supported gold nanoparticles for soot combustion: the metal-support interaction. J Catal 287:13–29
31. Kumar A, Babu S, Karakoti AS, Schulte A, Seal S (2009) Luminescence properties of europium-doped cerium oxide nanoparticles: role of vacancy and oxidation states. Langmuir 25: 10998–11007
32. Spanier JE, Robinson RD, Zheng F, Chan SW, Herman IP (2001) Size-dependent properties of CeO_{2-y} nanoparticles as studied by Raman scattering. Phys Rev B 64:245407–245415
33. Keramidast VG, White WB (1973) Raman spectra of oxides with the fluorite structure. J Chem Phys 59:1561–1562
34. Mandal S, Bando KK, Santra C, Maity S, James OO, Mehtad D, Chowdhury B (2013) Sm-CeO_2 supported gold nanoparticle catalyst for benzyl alcohol oxidation using molecular O_2. Appl Catal A 452:94–104
35. Patil S, Seal S, Guo Y, Schulte A, Norwood J (2006) Role of trivalent La and Nd dopants in lattice distortion and oxygen vacancy generation in cerium oxide nanoparticles. Appl Phys Lett 88:243110–243113
36. Parayanthal P, Pollak FH (1984) Raman scattering in alloy semiconductors: "spatial correlation" model. Phys Rev Lett 52: 1822–1825
37. Trogadas P, Parrondo J, Ramani V (2012) CeO_2 surface oxygen vacancy concentration governs in situ free radical scavenging efficacy in polymer electrolytes. ACS Appl Mater Interfaces 4:5098–5102
38. Nolan M (2012) Charge transfer and formation of reduced Ce^{3+} upon adsorption of metal atoms at the ceria (110) surface. J Chem Phys 136:134703–134711
39. Korsvik C, Patil S, Seal S, Self WT (2007) Superoxide dismutase mimetic properties exhibited by vacancy engineered ceria nanoparticles. Chem Commun 14:1056–1058
40. Aboukaïs A, Aouad S, El-Ayadi H, Skaf M, Labaki M, Cousin R, Abi-Aad E (2012) Physicochemical characterization of Au/CeO_2 solid. Part 1: the deposition–precipitation preparation method. Mater Chem Phys 137:34–41
41. Chen B, Shi C, Crocker M, Wang Y, Zhu A (2013) Catalytic removal of formaldehyde at room temperature over supported gold catalysts. Appl Catal B Environ 132:245–255